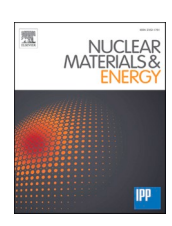
ELSEVIER

Contents lists available at ScienceDirect

Nuclear Materials and Energy

journal homepage: www.elsevier.com/locate/nme





Boron transport simulation using the ERO2.0 code for real-time wall conditioning in the large helical device

M. Shoji ^a, G. Kawamura ^{a,b}, J. Romazanov ^c, A. Kirschner ^c, A. Eksaeva ^c, D. Borodin ^c, S. Masuzaki ^{a,b}, S. Brezinsek ^c

- ^a National Institute for Fusion Science, National Institutes of Natural Sciences, 322-6 Oroshi-cho, Toki 509-5292, Japan
- ^b The Graduate University for Advanced Studies (SOKENDAI), Shonan Village, Hayama 240-0913, Japan
- c Forschungszentrum Jülich GmbH, Institut für Energie- und Klimaforschung Plasmaphysik, Partner of the Trilateral Euregio Cluster (TEC), Jülich 52425, Germany

ARTICLE INFO

Keywords: ERO2.0 Impurity powder dropper DUSTT EMC3-EIRENE LHD Boronization

ABSTRACT

The three-dimensional Monte-Carlo impurity transport and plasma surface interaction code ERO2.0 is applied to a full-torus model for the Large Helical Device (LHD). In order to find an optimum experimental condition for effective real-time wall conditioning (boronization) using an Impurity Powder Dropper (IPD), the toroidal and poloidal distribution of the boron flux density on the divertor components and the vacuum vessel are surveyed in various experimental conditions. The source profile of the neutral boron atoms originated from boron powders supplied from the IPD is calculated using the DUSTT code in background plasmas provided by the EMC3-EIRENE code. The simulations using ERO2.0 predict that higher plasma density operation is inappropriate for the effective wall conditioning because of the toroidally localized boron flux density in a closed helical divertor region. The ERO2.0 simulations have successfully revealed an optimum experimental condition for the wall conditioning with the toroidally uniform boron flux density in the closed helical divertor region.

1. Introduction

It is well known that wall conditioning is quite effective for high-performance plasma discharges by reducing the impurity radiation in the peripheral plasma, and the control of neutral particle recycling in the divertor region [1]. In the Large Helical Device (LHD), helium glow discharge cleaning (GDC) with diborane gas has been applied as a conventional wall conditioning (boronization) method performed a few times in one experimental campaign for these two decades [2]. One of the disadvantages of this conventional method is the difficulty of boron deposition in the closed helical divertor (CHD) region installed in the inboard side of the torus. This is because the CHD is located in a narrow area recessed from the GDC plasma, and the divertor plates in the CHD region do not directly face the GDC plasma.

In order to overcome this disadvantage, a wall conditioning method called "real-time boronization" was proposed [3]. This kind of technique has been recently applied to some Tokamaks [4–6]. An impurity powder dropper (IPD), which has been developed in the Princeton Plasma Physics Laboratory, was installed in one of the upper ports in the last experimental campaign in the fiscal year 2019 in LHD [7]. The boronization using the IPD was firstly tried and contributed to the reduction

of the impurity radiation to a certain extent [8]. The boron atoms contained in boron powders supplied from the IPD are evaporated and ionized in the peripheral plasma. The resultant boron ions are transported from the peripheral plasma to the divertor region along the magnetic field lines, which contributes to the deposition of boron in the divertor region and leads to an effective wall conditioning.

With a view to making full use of the IPD, an experimental condition which is appropriate for the effective wall conditioning has to be found in advance before this device will be routinely used hereafter. For this purpose, the three-dimensional Monte-Carlo impurity transport and plasma-surface interaction code ERO2.0 [9] was firstly applied to LHD. The ERO2.0 code calculates plasma wall interaction (PWI) processes such as reflection, physical/chemical sputtering, and deposition on the surface of the plasma facing components. The toroidal and poloidal distribution of the boron flux density on the surfaces of the divertor components and the vacuum vessel is calculated in various experimental conditions using a three-dimensional full-torus model for ERO2.0. In this simulation, the boron flux density gives a good indicator representing the growth rate of the boron layers deposited on the surface of the plasma facing components. It is expected that the simulations provide a useful guideline for realizing high-performance plasma discharges using

E-mail address: shoji@nifs.ac.jp (M. Shoji).

the IPD in future experimental campaigns.

2. Set up for the simulation of boron transport and deposition using ERO2.0 in the LHD

The LHD is one of the world's largest heliotron/stellarator type machines having super-conducting helical and poloidal coils to produce magnetic field configurations for confining a helically twisted shaped plasma without the toroidal plasma current. The major and averaged plasma minor radii are typically about 3.6 m and 0.6 m, respectively [10]. An ergodized magnetic field line structure is intrinsically formed in the peripheral plasma outside of the Last Closed Flux Surface (LCFS), which is called as an ergodic layer, and four bundled magnetic field lines (divertor legs) are formed in the divertor region. The magnetic field lines in the peripheral plasma (ergodic layer) are directly connected to the vacuum vessel (stainless steel) and divertor plates made of isotropic graphite (carbon).

The impurity transport and plasma-surface interaction simulations are performed using ERO2.0 in fixed pure deuterium background (BG) plasmas provided by a fully three-dimensional edge plasma simulation code (EMC3-EIRENE) [11,12]. In this code, fluid transport equations of peripheral plasmas along the magnetic field lines with perpendicular diffusion are solved by EMC3, and kinetic transport equations of neutral atomic and molecular processes are computed by EIRENE. The BG plasma parameter profiles in a full-torus grid model ($0^{\circ} < \phi < 360^{\circ}$ in toroidal direction ϕ) are created by toroidally extending the EMC3-EIRENE simulation results in one-half of the helical coil pitch angle $(0^{\circ} < \phi < 18^{\circ})$ with the assumption of up-and-down and toroidally periodic symmetries. The profiles are obtained from the calculations in an inward-shifted magnetic configuration in which the radial position of the magnetic axis R_{ax} equals to 3.60 m and the toroidal magnetic field direction is counter-clockwise. The EMC3-EIRENE code calculates the three-dimensional BG plasma parameter profiles under a boundary condition where the plasma heating power and the plasma density at an inner boundary locating just inside of the LCFS (P^{LCFS} and n_e^{LCFS}) respectively) are fixed to constant values. The perpendicular particle and the ion/electron thermal diffusion coefficients are assumed to be 0.5 and 1.0 m²/s, respectively, which are typical values for explaining the measured plasma density and temperature profiles in the peripheral plasma. It is assumed that the divertor components (closed helical divertor plates, dome plates, and open divertor plates) and the vacuum vessel have a 10-fold toroidal periodicity. An open divertor structure in one helical section in the actual configuration is not included in this fulltorus model. The divertor components and the vacuum vessel in this model consist of the groups of small triangle surfaces being less than a few cm in length. The materials consisting of the divertor components and the vacuum vessel are treated as carbon and iron, respectively.

The three-dimensional distribution of an impurity source (neutral boron atoms) has to be defined for ERO2.0 as an input parameter for the impurity transport simulation. The distribution of the neutral boron atoms originating from the boron powders supplied from the IPD is provided by a dust transport simulation code (DUSTT) [13-15]. The DUSTT code solves the equation of motion of a spherical shaped powder coupled with the heat, charge, mass equations including the effect of the ion/neutral drag force, gravity force, electrostatic force. A pure boron powder is injected downward with a velocity of 5.0 m/s from an initial position located in a grid model for the one-half of the helical coil pitch angle (0° $\leq \phi \leq 18^{\circ}$) which is specially prepared for calculating the three-dimensional trajectory of the boron powder dropped from the IPD installation position. The downward velocity approximately corresponds to the falling speed at the initial position on the free fall trajectory. Because the IPD is installed in an upper port in a helical section with the open divertor structure, the CHD components are not included in this grid model. The DUSTT code calculates the three-dimensional trajectory of the boron powder in a fixed BG plasma with the parameter profiles (the plasma density and the ion/electron temperature, the plasma flow velocity and so on) provided by EMC3-EIRENE in which the impurity (carbon) is eliminated for the simple calculation. When the boron powder reaches the peripheral plasma, the temperature of the boron powder rises by the heat load from the plasma, and the temperature finally reaches the boiling point. The distribution of the source profile of the neutral boron atoms is defined as the boron evaporation rate at the positions along the powder trajectory. Although the EMC3-EIRENE code can provide the toroidal and poloidal distribution of the boron ion flux densities on the plasma facing components [16], the code does not include sophisticated database on plasma wall interactions. The reflection of the incident ions, and the physical/chemical sputtering of target atoms are coarsely simplified in EMC3-EIRENE which promoted us to fully apply the ERO2.0 to the detailed analysis of the full-torus distribution of the boron flux density in LHD.

Fig. 1 illustrates a perspective view of the three-dimensional grid model for calculating the boron powder trajectories. The initial position for tracking the powders is indicated as a small yellow circle close to an upper divertor leg. An outlet for dropping the powders is installed above $\sim\!2$ m from the initial position. The gravity acts in the –Z direction (downward). A poloidal cross-section of the grids for the peripheral plasma (the ergodic layer and the divertor legs) is shown, which is the cross-section at a toroidal angle ϕ of –6.125° at which the IPD is installed (the LHD plasma is vertically elongated at $\phi=0^\circ$). Typical plasma density and electron temperature at the divertor legs are in the order of 10^{18} m $^{-3}$ and around 30 eV, respectively. Higher density and temperature plasmas are formed in the ergodic layer surrounding the core plasma.

The three-dimensional source profile of the neutral boron atoms is one of the essential parameters for investigating the performance of the wall conditioning using the IPD. Thus, the boron powder trajectory in the peripheral plasma in various experimental conditions are surveyed by changing the plasma density $n_{\rm e}^{\rm LCFS}$, the boron powder size (diameter) $d_{\rm B}$, and the plasma heating power $P^{\rm LCFS}$. Fig. 2 (a) gives the trajectories for two different plasma densities ($n_{\rm e}^{\rm LCFS}=1\times10^{19}~{\rm m}^{-3}$ and 4×10^{19} m^{-3} with $P^{LCFS} = 8$ MW) for a powder diameter d_B of 150 μ m. The position of the area displayed in this figure is shown as a red broken square in Fig. 1. The points where the boron powders are completely evaporated are indicated as open white circles as a good indicator for representing the penetration of the powders into the plasma. It should be noted that the neural boron atoms are distributed along the powder trajectories to the evaporation positions. The boron evaporation rate along the powder trajectories is shown as coloured dots in Fig. 2. The trajectories show that the boron powders have to pass through the upper divertor leg before reaching the ergodic layer. For the higher plasma density ($n_e^{\text{LCFS}} = 4 \times 10^{19} \text{ m}^{-3}$), the trajectory is considerably deflected at the divertor leg due to the effect of the plasma flow (the ion drag force directed from the ergodic layer to the divertor plates as shown an arrow in Fig. 2 (a)), which results in the evaporation position at the outer edge of the ergodic layer. Compared to the high plasma density case, the evaporation position for the low plasma density ($n_e^{LCFS} = 1 \times 10^{19} \text{ m}^{-3}$) is located in the deeper region in the ergodic layer, which is thanks to the smaller deflection of the trajectory because of the lower ion drag force in the divertor leg due to the lower divertor plasma density. These simulation results are consistent with the recent spectroscopic measurements of the intensity ratio of boron ions (BV and BII) in high and low plasma densities, indicating that the boron powder reaches the ergodic layer and produces the boron ions more effectively for the lower plasma density [8].

The calculated boron powder trajectories for various powder sizes d_B are presented in Fig. 2 (b), in which the plasma density n_e^{LCFS} and the heating power P^{LCFS} are set to be $1\times 10^{19}~\text{m}^{-3}$ and 8 MW, respectively. The powder size is changed from 100 μm to 200 μm in diameter (the nominal maximum tolerable diameter is 200 μm for the IPD). Larger powders tend to penetrate into the deeper region in the ergodic layer. The larger the powder size is, the more the evaporated position approaches the core plasma, which is because the increment of the powder

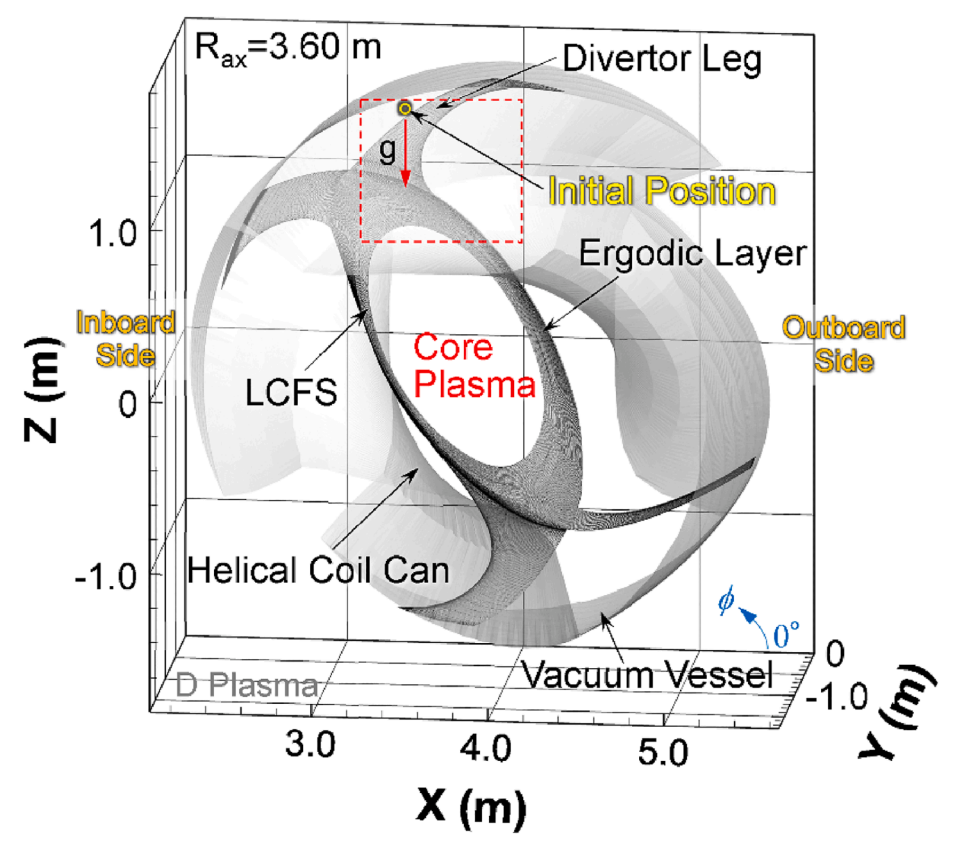


Fig. 1. A perspective view of a three-dimensional grid model for the one-half of the helical coil pitch angle ($0^{\circ} \leq \phi \leq 18^{\circ}$) for calculating the trajectory of boron powders dropped from the IPD. An open yellow circle indicates the initial position for tracking the trajectories. This model includes the structure of the vacuum vessel and the LHD peripheral plasma (the ergodic layer and the divertor legs). The poloidal cross-section of the grids for the peripheral plasma at the toroidal angle, at which the IPD is installed, is also presented. (For interpretation of the references to colour in this figure legend, the reader is referred to the web version of this article.)

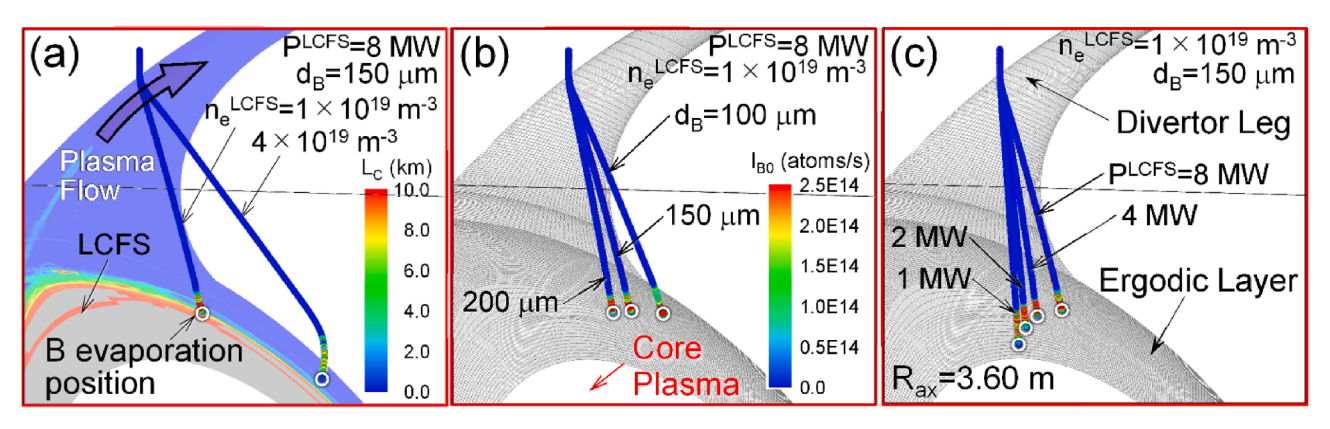


Fig. 2. The calculations of the dropped boron powder trajectories in the case of the low and high plasma densities $(n_e^{\rm LCFS} = 1 \times 10^{19} \ {\rm m}^{-3})$ and $4 \times 10^{19} \ {\rm m}^{-3}$, respectively). The poloidal cross-section of the connection length of the magnetic field lines $L_{\rm C}$ in the peripheral plasma is presented (the grey area indicates the region where the connection length is more than 10 km). (b) The calculated boron powder trajectories for three different powder sizes $d_{\rm B}$ in the range from 100 μm to 200 μm. The poloidal cross-section of the grid meshes of the LHD peripheral plasma is illustrated. (c) The trajectories for four different plasma heating powers $P^{\rm LCFS}$ in the range from 1 MW to 8 MW. The colour on the trajectories indicates the boron evaporation rate (the contour legend is shown in Figure (b)). The positions where the boron powders are completely evaporated are indicated as open white circles. The boron powder for the high plasma density ($n_e^{\rm LCFS} = 4 \times 10^{19} \ {\rm m}^{-3}$) in Figure (a) appears to be evaporated in the outside of the ergodic layer because of the different toroidal positions of the boron powder.

temperature becomes smaller due to the larger heat capacity. The deflection of the dropping trajectories of the larger sized powders at the upper divertor leg is more moderate, which is thanks to the inertia of the heavier (larger) powders. These two contribute to moving the evaporation position of the boron powders to a higher plasma temperature region close to the core plasma.

DUSTT simulations show that the trajectories of the boron powders which sizes are smaller than 100 μm cannot reach the ergodic layer by the deflection of the dropping trajectories at the divertor leg. This result indicates that a minimum inertia (powder size) is necessary for the boron powders to provide evaporated boron atoms in the peripheral

plasma. The deflection of the trajectories was investigated in a parameter space (1 \times $10^{19}~m^{-3} \leq n_{\rm e}^{\rm LCFS} \leq 8 \times 10^{19}~m^{-3}$ and 1 MW $\leq P^{\rm LCFS} \leq 8$ MW) in different powder sizes from 2 μm to 200 μm in diameter. The DUSTT simulations show that the higher plasma heating power enhances the deflection of the trajectories which is caused by the increased plasma flow velocity due to the plasma temperature rise in the divertor leg. It is found that this effect is smaller than that by the plasma density rise, which means that the enhanced plasma flow velocity by the plasma heating is just a side effect for increasing the ion drag force. The simulation reveals that smaller sized powders are inapplicable to the production of the evaporated boron atoms in the peripheral plasma in all

parameter ranges (n_e^{LCFS} and P^{LCFS}).

Fig. 2 (c) presents boron powder trajectories for four different plasma heating powers $P^{\rm LCFS}$ under the condition where the plasma density $n_{\rm e}^{\rm LCFS}$ is $1\times 10^{19}~{\rm m}^{-3}$ and the powder size $d_{\rm B}$ is 150 $\mu{\rm m}$. The evaporation positions of the boron powders are drastically changed with the plasma heating power. The lower the plasma heating power is, the more the evaporated position approaches the core plasma because of the lower plasma heat load on the powders which make the powders penetrate into the deeper region in the peripheral plasma.

The neutral boron atoms released from the evaporated boron powders are tracked by ERO2.0 in the full-torus model. In this simulation, test particles, which represent the boron atoms, are released with a kinetic energy corresponding to the boiling point. The direction of the test particles is randomly chosen from the isotropic distribution. A large number (in the order of one million) of test particles are launched from the birth points of the evaporated boron atoms along the trajectories. The weighting ratio of the number of the test particles is in proportion to the boron evaporation rate calculated by the DUSTT at the birth points, in which the trajectory of a single boron powder is tracked using this code for calculating the distribution of the neutral boron atoms. In this simulation, the dropping rate of the numbers of the boron atoms contained in the powders is set to be 6.24×10^{15} atoms/s which is found to be too small to perturb the BG plasmas [16]. Most of test particles released from the boron powders are ionized in the plasma. The ionization/recombination rates of the boron atoms/ions are derived from the database on the Atomic Data and Analysis Structure (ADAS) [17]. The ERO2.0 code tracks boron ion trajectories with a diffusion coefficient of 1.0 m²/s which provides the most reasonable simulation results of an impurity (carbon) being compatible with both observed line emission ratios and the absolute line emission in the past [18]. When the test particles (boron ions) enter the inner boundary of the grid model, new test particles are regenerated at random positions on the surface at the inner boundary. This is an adequate measure for simulating the impurity transport in the core plasma because of the formation of the nested magnetic flux surfaces in this region.

The boron atoms/ions colliding with the plasma facing components such as the vacuum vessel and the divertor plates are deposited or reflected on the surfaces. The boron atoms/ions induce the physical and chemical sputtering on the components. The angular and the energy dependences of the reflection coefficients and sputtering yields are provided by simulations using the SDTrimSP code for specified projectile-target combinations (boron on carbon and boron on iron) [19]. The ERO2.0 simulation provides a time-dependent solution such as the boron flux density on the plasma facing components. The erosion of the deposited boron induced by the plasma (deuterium ion) and by the sputtered carbon/iron atoms released from the plasma facing components is not included in this simulation. The re-deposition of the eroded boron and the boron self-sputtering are not considered for the simplicity, meaning that the simulation corresponds to a so-called "the first time step calculation" in ERO2.0. Including these effects may broaden the toroidal and poloidal distribution of the boron flux density because of the boron transport from high boron flux areas. Inclusion of these effects is planned for a future work.

3. Full-torus boron transport simulation for finding an optimum plasma discharge condition for effective wall conditioning

In order to find an optimum experimental condition for effective wall conditioning using the IPD, full-torus boron transport simulations were performed using ERO2.0 in various experimental conditions. Fig. 3 is a perspective view of a simulation result of the full-torus distribution of the boron flux density on the surfaces of the divertor components (the vacuum vessel is not shown in this figure). In this simulation, the boron powder size $d_{\rm B}$ is 150 µm in diameter, the plasma density $n_{\rm e}^{\rm LCFS}$ is 4 ×

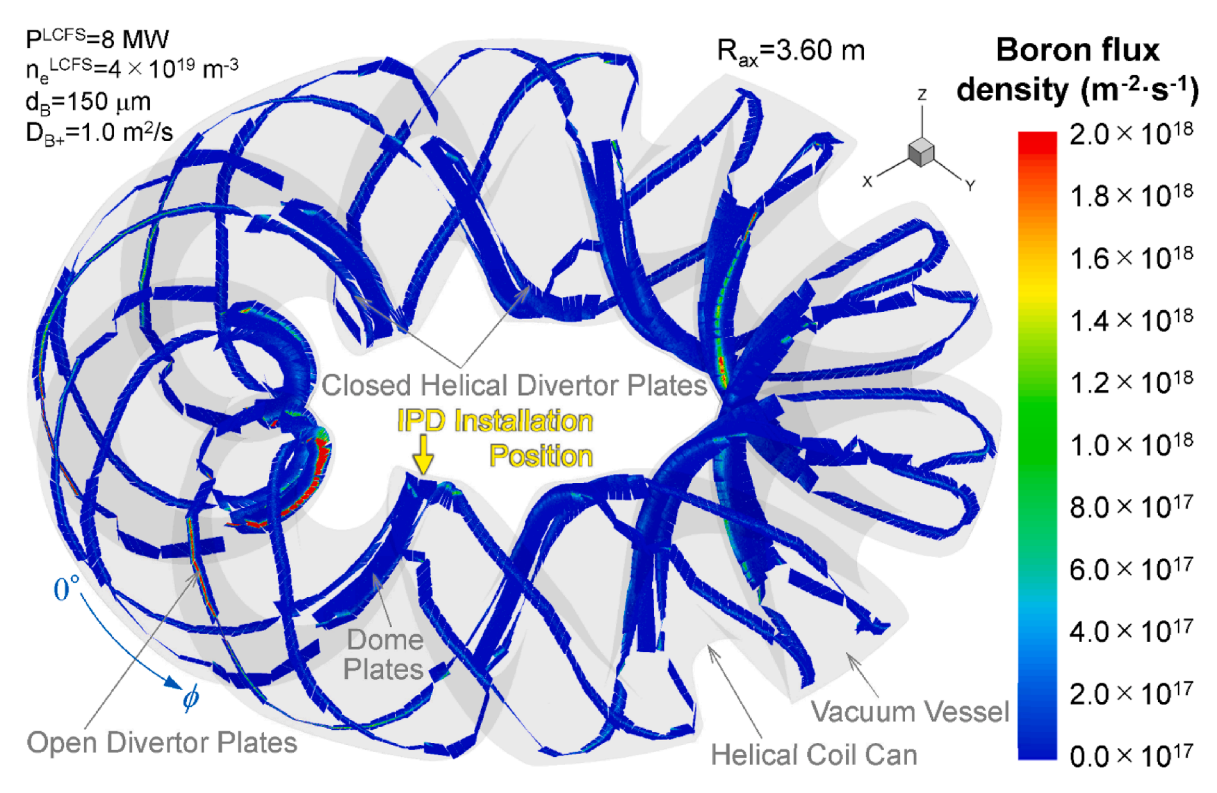


Fig. 3. A perspective view of the simulation result of the full-torus toroidal and poloidal distribution of the boron flux density on the divertor components. The shape of the vacuum vessel is displayed as semi-transparent surfaces. The boron deposition on the vacuum vessel and that on the back plates of the divertor components are not shown. It should be noted that the boron flux density on the front surfaces of the divertor components can be seen from the backside. The IPD installation position is approximately indicated as a yellow arrow. (For interpretation of the references to colour in this figure legend, the reader is referred to the web version of this article.)

 $10^{19}~{\rm m}^{-3}$, and the plasma heating power $P^{\rm LCFS}$ is set to be 8 MW. The colour on the divertor components indicate the flux density of the boron atoms. It should be noted that the back plates of the divertor components are not displayed in this figure, which means that the boron flux density on the front surfaces of the divertor components is seen from the backside. This figure shows that while the boron is distributed along the strike points (the plasma wetted areas) on the divertor plates, the toroidal distribution of the boron flux density is not uniform. That is, the boron flux density on the closed helical divertor plates in the inboard side installed in a helical section adjacent to the IPD installation position is considerably higher than that in the other helical sections. This extremely localized boron flux density is unfavourable for effective wall conditioning for reducing impurities in LHD plasmas.

For finding an optimum experimental condition for achieving toroidally uniform boron flux density especially in the CHD region, the following three parameters are surveyed: the plasma density $n_{\rm e}^{\rm LCFS}$, the boron powder size $d_{\rm B}$, and the plasma heating power $P^{\rm LCFS}$. The boron flux density is displayed on the full-torus toroidal and poloidal plane as a two-dimensional grey-scale plot. Fig. 4 (a) and (b) show the simulations of the boron flux density distribution for low and high plasma densities ($n_{\rm e}^{\rm LCFS}=1\times10^{19}~{\rm m}^{-3}$ and $4\times10^{19}~{\rm m}^{-3}$ with $P^{\rm LCFS}=8$ MW and $d_{\rm B}=150~{\rm \mu m}$), respectively. The boron flux density on the dome plates is not displayed in the figures. A small yellow circle approximately indicates the initial position for tracing the boron powder trajectories by DUSTT projected onto the toroidal and poloidal plane. The two figures indicate that, in the high plasma density case, the flux density is locally high (a) compared to that in the low plasma density case (b). For the high plasma

density, the boron flux density is extremely high in the CHD region where the poloidal angle θ is in the range $120^{\circ} \le \theta \le 240^{\circ}$ with a toroidal angle of around 342°. This position corresponds to the helical section where the boron flux density is extremely high in the CHD region in Fig. 3. This localization is due to the high boron ion flux from the evaporation position of the boron powders in an adjacent helical section. As shown in Fig. 2 (a), the boron powders generate the source of neutral boron atoms in the outer edge of the ergodic layer where the connection length of the magnetic field lines $L_{\mathbb{C}}$ is very short (in the order of several meters) [20]. It means that, for the high plasma density, most of the resultant boron ions are transported to the adjacent CHD region along the magnetic field lines. In addition to this, the CHD region is surrounded by the divertor components such as the inclined divertor plates and the dome plates in a narrow space, which increases the boron flux density caused by the reflected and sputtered boron atoms in this region [21]. Additionally, the ERO2.0 simulation clarifies that the boron flux density is quite high on the surface of a helical coil can in the inboard side (the poloidal angle $\theta \sim 180^{\circ}$) at a toroidal angle of around 324° (close to the CHD region). This is because the helical coil can is extruded from the inner surface of the vacuum vessel toward the plasma, leading to the additional boron flux on the helical coil can. The simulation results using ERO2.0 reveals that the plasma discharge operation with the high n_e^{LCFS} is inappropriate for the effective wall conditioning with the toroidally uniform boron flux density. The simulation shows that the evaporation position of the boron powders definitely influences the toroidal and poloidal distribution of the boron flux density. This result indicates that the ion drag force in the divertor legs should be reduced as

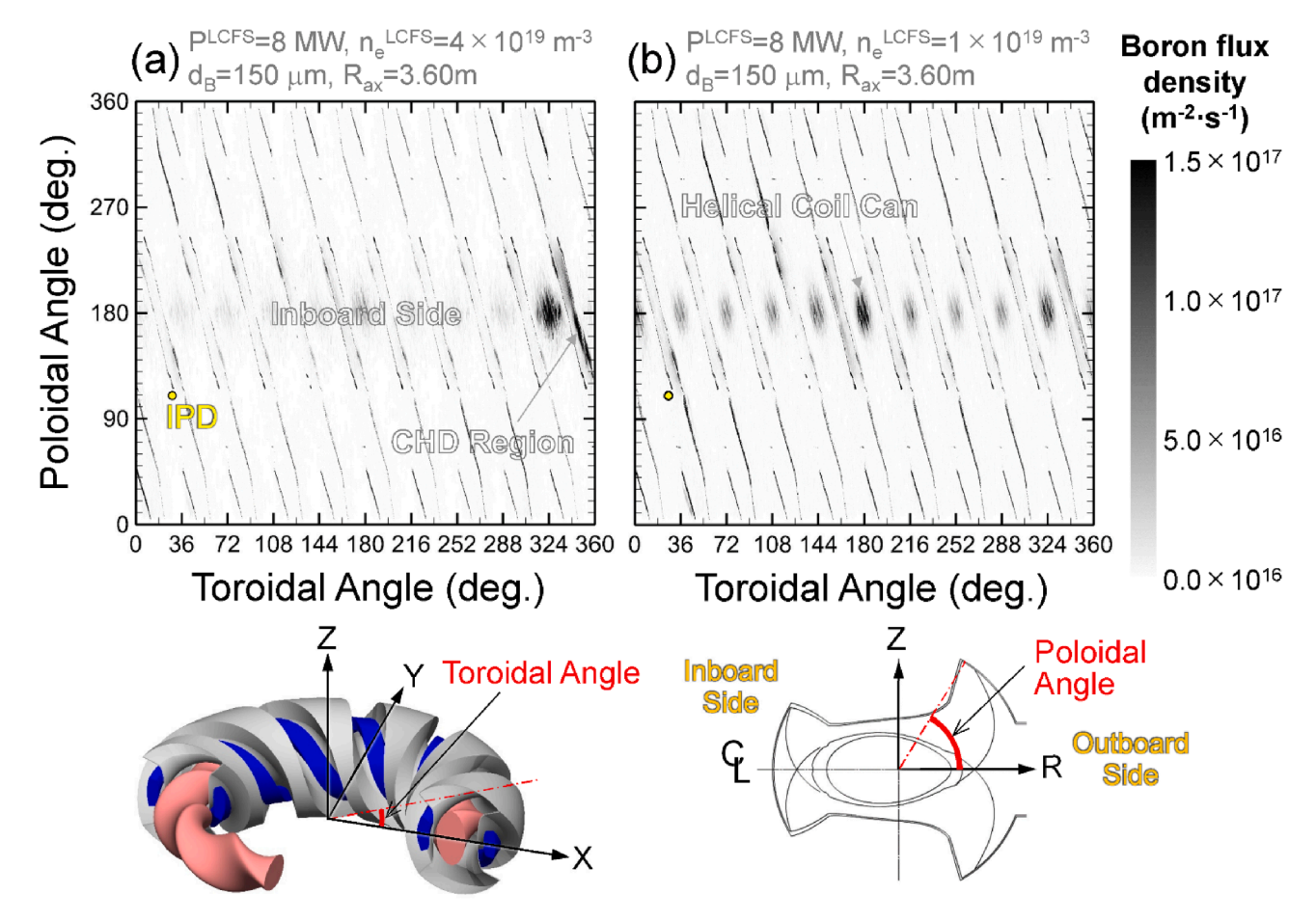


Fig. 4. The grey scale plot of the calculated boron flux density distribution projected onto the full-tours toroidal and poloidal plane. The boron flux density on the surface of the divertor components and the vacuum vessel is displayed for $n_e^{\rm LCFS} = 1 \times 10^{19} \, {\rm m}^{-3}$ (a) and $4 \times 10^{19} \, {\rm m}^{-3}$ (b), respectively. The inboard side of the torus corresponds to the areas where the poloidal angle is around 180° . The boron flux density on the dome plates is not shown in this figure. The initial position for tracing the boron powder trajectories projected on the plane is approximately indicated as a small yellow circle. (For interpretation of the references to colour in this figure legend, the reader is referred to the web version of this article.)

much as possible. Since it has been found that the plasma density in the divertor legs are strongly correlates with that in the ergodic layer because of the short connection length of the magnetic field lines (less than a few meters) in the divertor legs [22], the control of the peripheral plasma density, which is a dominant factor for changing the ion drag force, is essential for making full use of the IPD for the wall conditioning.

It is expected that the increase in the boron powder size can contribute to more toroidally uniform boron flux because larger boron powders are fully evaporated in the deeper region in the peripheral plasma where the connection length $L_{\rm C}$ is much longer [20], by which the resultant boron ions can be transported to the divertor region locating far from the IPD installation position. Fig. 5 (a) and (b) display the boron flux density distribution for two powder sizes ($d_{\rm B}=100~\mu {\rm m}$ and 200 $\mu m)$ under the low plasma density $n_e^{LCFS} = 1 \times 10^{19} \ m^{-3}$ with $P^{\text{LCFS}} = 8$ MW, respectively. In both cases, the calculated boron flux density on the helical coil can in the inboard side of the torus is relatively high at toroidal angles of 180° and 324° . The boron flux density in the CHD region next to these two toroidal angles ($\theta \sim 162^{\circ}$ and 342°) is also higher than that at the other toroidal angles. The simulations suggest that the increase in the powder size is not so effective for improving the toroidal uniformity of the boron flux density in the divertor region. One of the reasons for the insignificant difference of the boron flux density distribution in both powder sizes is attributed to the roughly equivalent source profile of neutral boron atoms along the trajectories in the ergodic layer where the L_C is relatively short in the both cases. By the above simulation results, the ERO2.0 code demonstrates that the increase in the powder size in the range between 100 μm and 200 μm is not appropriate for performing effective wall conditioning using the IPD.

The change of the plasma heating power drastically affects the evaporation position of the boron powders as shown in Fig. 2 (c). Lower plasma heating powers are expected to be appropriate for achieving more toroidally uniform boron flux distribution in the divertor region because the evaporated position in lower heating powers is close to the core plasma where the connection length L_C is very long (more than10 km). Fig. 6 (a) and (b) display the simulations of the boron flux density distribution for two low plasma heating powers ($P^{\rm LCFS}=2$ MW and 1 MW) under the condition of the low plasma density $n_{\rm e}^{\rm LCFS}=1\times 10^{19}\,{\rm m}^{-3}$ with $d_{\rm B}=150~{\rm \mu m}$, respectively. Compared to the profile for the high plasma heating power ($P^{\rm LCFS}=8$ MW) as shown in Fig. 4 (a), the toroidal uniformity of the boron flux density in the divertor region and on the

helical coil can is significantly improved, where the flux density on the helical coil can at the two toroidal angles (180° and 324°) is not considerably higher than that at the other helical coil cans. The ERO2.0 simulations predict that the lower plasma heating power operation ($P^{\text{LCFS}} \leq 2$ MW) is effective for improving the toroidal uniformity of the boron flux density in the divertor region and on the helical coil cans, which is favourable for the effective wall conditioning using the IPD as far as the plasma is not terminated by the radiation collapse [23]. Especially, long pulse discharges with lower plasma densities are appropriate for the wall conditioning, which enables the IPD to continuously supply the boron powders to the LHD peripheral plasma.

4. Summary

In order to find an optimum experimental condition for effective wall conditioning (boronization) using the IPD, full-torus boron transport simulation was performed using ERO2.0 under background plasmas calculated by EMC3-EIRENE coupled with the source profile of the neutral boron atoms provided by DUSTT. The full-torus toroidal and poloidal distribution of the boron flux density is calculated in various experimental conditions by changing the following three parameters: the plasma density $n_{\rm e}^{\rm LCFS}$, the boron powder size (diameter) $d_{\rm B}$, and the plasma heating power $P^{\rm LCFS}$. The simulations show that the higher plasma density ($n_e^{LCFS} = 4 \times 10^{19} \text{ m}^{-3}$) is undesirable for achieving toroidally uniform boron flux density in the divertor region and on the helical coil can. This is because the boron evaporation position locates in the outer edge of the ergodic layer, which is caused by the significant deflection of the boron powder trajectory at the upper divertor leg due to the ion drag force caused by the plasma flow from the ergodic layer to the divertor plates. The control of the plasma density, which is a dominant factor for the ion drag force, is essential for making full use of the IPD. The simulation also indicates that the increase in the powder size is not effective for improving the toroidal uniformity of the boron flux density. The ERO2.0 code predicts that the lower plasma heating power ($P^{LCFS} \leq 2$ MW) with the low plasma density ($n_e^{LCFS} = 1 \times 10^{19}$ m^{-3}) is quite effective for achieving the toroidally uniform boron flux density, which can contribute to the effective real-time wall conditioning for sustaining high-performance plasma discharges in LHD.

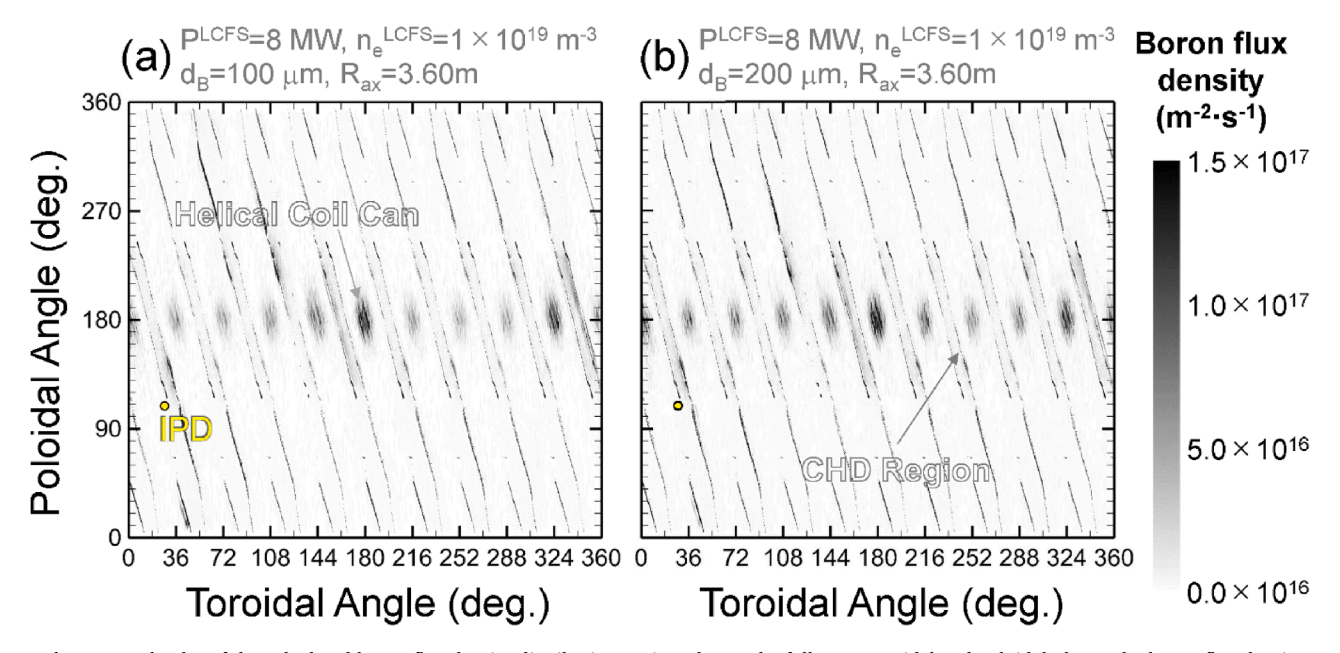


Fig. 5. The grey scale plot of the calculated boron flux density distribution projected onto the full-tours toroidal and poloidal plane. The boron flux density on the surface of the divertor components and the vacuum vessel is illustrated for the boron powder sizes d_B of 100 μ m (a) and 200 μ m (b), respectively.

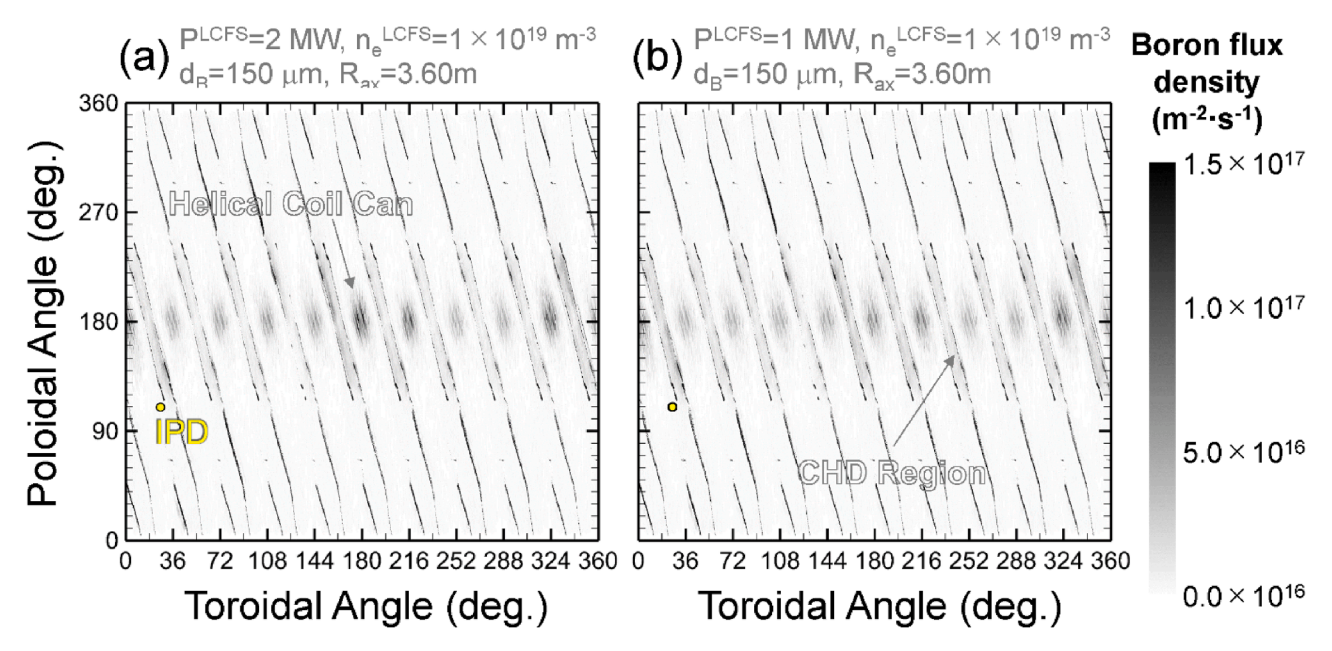


Fig. 6. The grey scale plot of the calculated boron flux density distribution projected onto the full-tours toroidal and poloidal plane. The boron flux density on the surface of the divertor components and the vacuum vessel is shown for the two plasma heating powers P^{LCFS} of 2 MW (a) and 1 MW (b), respectively.

CRediT authorship contribution statement

M. Shoji: Supervision, Investigation, Writing - original draft, Visualization. G. Kawamura: Software, Resources. J. Romazanov: Software, Writing - review & editing. A. Kirschner: Software, Project administration. A. Eksaeva: Software. D. Borodin: Software. S. Masuzaki: Conceptualization, Supervision, Project administration, Funding acquisition. S. Brezinsek: Project administration.

Declaration of Competing Interest

The authors declare that they have no known competing financial interests or personal relationships that could have appeared to influence the work reported in this paper.

Acknowledgments

This work is performed under the auspices of the NIFS Collaboration Research program (NIFS12KNXN236). The author would like to thank Y. Feng for permission to use the EMC3-EIRENE. He is also grateful to Profs. S. I. Krasheninnikov and Y. Tanaka, and Dr. R. D. Smirnov for providing the DUSTT, and for the support for using the code in our computational environment. Furthermore, he appreciates the computational resources of the LHD numerical analysis server and the plasma

simulator in NIFS. This work is also supported by JSPS KAKENHI Grant Numbers 18H01203, 16H04619, and 16K18340.

References

- [1] J. Winger, et al., Plasma Phys. Control. Fusion 38 (1996) 1503.
- [2] K. Nishimura, et al., J. Nucl. Mater. 337 (2005) 431.
- [3] A. Sagara, et al., J. Nucl. Mater. 241-243 (1997) 972.
- [4] A. Bortolon, et al., Nucl. Mater. Energy 19 (2019) 384.
- [5] R. Lunsford, et al., Nucl. Fusion 59 (2019), 126034.
- [6] A. Bortolon, et al., Nucl. Fusion 60 (2020) 126010.[7] A. Nagy, et al., Rev. Sci. Instrum. 89 (2018) 10K121.
- [8] N. Federico et al., These proceedings for PSI2020.
- [9] J. Romazanov, et al., Nucl. Mater. Energy 18 (2019) 331.
- 10] Y. Takeiri, et al., Nucl. Fusion 57 (2017), 102023.
- [11] Y. Feng, et al., Plasma Phys. Control. Fusion 44 (2002) 611.
- [12] G. Kawamura, et al., Contrib. Plasma Phys. 54 (2014) 437.
- [13] A.Y. Pigarov, et al., J. Nucl. Mater. 363-365 (2007) 216.
- [14] R.D. Smirnov, et al., Plasma Phys. Control Fusion 49 (2007) 347.
- [15] Y. Tanaka, et al., J. Nucl. Mater. 415 (2011) S1106.
- [16] M. Shoji, et al., Contrib. Plasma Phys. 60 (2020), e201900101.
- [17] The ADAS User Manual (version 2.6) http://adas.phys.strath.ac.uk/ (2004).
- [18] S. Dai, et al., Nucl. Fusion 56 (2016), 066005.
- [19] W. Möller, et al., Comput. Phys. Commun. 51 (1988) 355.
- [20] T. Watanabe, et al., Nucl. Fusion 46 (2006) 291.
- [21] M. Shoji, et al., Contrib. Plasma Phys. 56 (2016) 651.
- [22] S. Masuzaki, et al., Nucl. Fusion 42 (2002) 750.
- [23] B.J. Peterson, et al., Phys. Plasmas. 8 (2001) 3861.